Development of Many−Body Polarizable Force Fields for Li-Battery Applications: 2. LiTFSI-Doped Oligoether, Polyether, and Carbonate-Based Electrolytes

Oleg Borodin*,† and Grant D. Smith†,‡

Department of Materials Science & Engineering, 122 South Central Campus Drive, Room 304, University of Utah, Salt Lake City, Utah 84112, and Department of Chemical Engineering, University of Utah, Salt Lake City, Utah 84112

Received: September 8, 2005; In Final Form: January 3, 2006

A quantum chemistry study of Li^+ interactions with ethers, carbonates, alkanes, and a trifluoromethanesulfonylimide anion ($TFSI^-$) was performed at the MP2, B3LYP, and HF levels using the aug-cc-pvDz basis set for solvents and $TFSI^-$ anion, and [8s4p3d/5s3p2d]-type basis set for Li. A classical many-polarizable force field was developed for the LiTFSI salt interacting with ethylene carbonate (EC), γ-butyrolactone (GBL), dimethyl carbonate (DMC), acetone, oligoethers, *n*-alkanes, and perfluoroalkanes. Molecular dynamics (MD) simulations were performed for EC/LiTFSI, PC/LiTFSI, GBL/LiTFSI, DMC/LiTFSI, 1,2-dimethoxyethane/LiTFSI, pentaglyme/LiTFSI, and poly(ethylene oxide) (MW = 2380)/LiTFSI electrolytes at temperatures from 298 to 423 K and salt concentrations from 0.3 to 5 M. The ion and solvent self-diffusion coefficients, electrolyte conductivity, electrolyte density, LiTFSI apparent molar volumes, and structure of the Li^+ cation environment predicted by MD simulations were found in good agreement with experimental data.

I. Introduction

Lithium-ion secondary batteries with liquid and gel electrolytes are currently used in the majority of portable electronic devices and are main candidates for use in environmentally friendly and efficient hybrid-electric vehicles (HEV).[1] Traditional liquid electrolytes are based on a mixture of cyclic carbonates and ethers. They have high-bulk conductivity, but also possess high volatility, and no mechanical stability requiring the presence of a separator to prevent electrode contact. Lithium-metal batteries with poly(ethylene oxide)-based polymeric electrolytes promise improved mechanical and electrochemical stability, low flammability and toxicity, and are potential candidates for use in rechargeable lithium batteries including HEV applications. However, low ionic conductivities and transference number of polymer electrolytes at ambient temperatures result in a significant deterioration of battery performances. Gel electrolytes formed from polymer electrolytes by the addition of 10−25% of plasticizer to the SPEs exhibit conductivities 5−10 times[2,3] higher than their traditional SPE counterparts. Further addition of additives up to 60−80% results in gel electrolytes that can reach conductivities only 1−2 orders of magnitude lower than liquid electrolytes.[4−6] The price to pay for the increased ion transport is poor mechanical properties and increased solvent volatility, especially at high plasticizer concentrations. A fundamental understanding of ion transport in liquid, gel, and SPE electrolytes is expected to assist in guiding new electrolyte design. Molecular dynamics (MD) simulations are, in principle, well suited for exploring transport mechanisms in liquid, gel, and polymer electrolytes, provided that the force field used is accurate enough for the prediction of the properties of interest.

Previous Non-Aqueous Electrolyte Simulations Containing Li-salts. A survey of the ability of MD previous simulations[7,8] of Li-salt in carbonate and oligoether-based solvents indicated mixed successes. One of the successes of using two-body force fields for understanding the electrolyte structure is reflected in MD simulations using an AMBER-based ether/Li-triflate force field to predict a fraction of free anions (i.e., anions not complexed by Li^+) and ion aggregates in the tetraglyme/Li-triflate electrolyte observed in IR experiments[9] as a function of temperature. There was a caveat, however, in the analysis of the simulations results. Specifically, a number of Li^+ around a triflate anion was calculated by integration from zero to the maximum of the Li−O radial distribution function. If the usual procedure for quantifying anion−cation complexes, such as integration of the whole first peak of the Li−O radial distribution function, was used, MD simulations would predict much larger cation−anion aggregation than the experimentally observed one. In another simulation study of liquid electrolytes, Tasaki[10] investigated a tendency of $LiPF_6$ salt to dissociate during 200 ps in various ether and carbonate-based solvents and found that the average $Li^+\cdots P$ distances in various solvents observed in his simulations were consistent with some experimental data on $LiPF_6$ dissociation, but equilibrium ion association constants were not calculated in the simulations.

Unfortunately, only a few groups reported the conductivity of Li-salt electrolytes as a function of salt concentration, because the long ($\sim 10^{-8}-10^{-9}$ s) simulation times required to obtain converged results make simulations rather computationally expensive. The PC/$LiBF_4$ simulations yielded conductivity[11] by a factor of 5−10 lower than experiments. Conductivity of PEO/LiI from MD simulations by Müller-Plather et al.[12] was approximately an order of magnitude higher than the expected experimental values after authors decreased all electrostatic interactions by a factor of 3 to observe any ion motion on a nanosecond time scale. MD simulations[13] using an nonpolar-

* To whom correspondence should be addressed. E-mail: borodin@eng.utah.edu.
† Department of Materials Science & Engineering.
‡ Department of Chemical Engineering.

10.1021/jp055080d CCC: $33.50 © 2006 American Chemical Society
Published on Web 03/04/2006

izable poly(ethylene oxide) (PEO)/NaI force field predicted unphysical phase separation where a miscible system was expected. However, a rather accurate, e.g., better than a factor of 2, prediction the Li^+ self-diffusion coefficient at infinite dilution in liquid electrolytes was obtained using two-body force fields.[7,8]

In our previous work,[14] we utilized polarizable force fields for PEO/Li-salt electrolytes. Quality of ion transport prediction from MD simulations improved from an order of magnitude estimates from simulations using effective two-body force fields[15] to a factor of 2−3 as many-body polarizable interactions were included in the force fields. In this contribution, we develop and validate classical many-body polarizable force fields for simulations of a number of most popular and widely investigated liquid electrolytes (ethylene carbonate (EC), propylene carbonate (PC), dimethyl carbonate (DMC), 1,2-dimethoxy ethane (DME), γ-butyrolactone (GBL), etc) and polymer electrolytes doped with lithium bis-trifluoromethanesulfonylimide $Li(CF_3SO_2)_2N$ (LiTFSI) salt. The LiTFSI salt was chosen as it is one of the most promising salts that has a significant charge delocalization resulting in a high fraction of salt dissociation (high fraction of free ions) and, therefore, high conductivities. Transferable many-body polarizable force fields for solvents from the preceding paper[16] are combined with the Li^+/solvent parameters developed in Section 3 on the basis of quantum chemistry calculations summarized in Section 2. Thermodynamic, structural, and transport properties of electrolytes from MD simulations are compared with experimental data in Section 4.

II. Quantum Chemistry Studies of the Li^+/Solvent and Li^+/$TFSI^-$ Complexes

In this section, we establish levels of theory that are adequate for accurate prediction of the Li^+/solvent and Li^+/$TFSI^-$ binding energies. Following previous studies[17] of the LiI, LiCl, and Li^+/ether binding, a Li^+ basis set of the [8s4p3d/5s3p2d] type with an improved description of 1s is used exclusively for all Li^+ computations reported in this contribution. Only solvent and anion basis sets need to be determined.

In this study, we utilize an augmented correlation consistent double-ζ (aug-cc-pvDz) basis set because previous quantum chemistry calculations[18] at the B3LYP level employing the aug-cc-pvDz basis set adequately described Coulomb and polarization interactions of a number of small organic molecules. However, the aug-cc-pvDz basis set is known to underestimate anion polarizability, and the usage of doubly and triply augmented basis sets is required for an accurate polarizability prediction of anions.[19] For example, the MP2/aug-cc-pvDz level calculations yielded a polarizability of Cl^- of 62% at the extrapolated augmentation limit at the CCSD(T) level.[19] Interestingly, polarizability of the same Cl^- anion solvated in water was found 63% of its gas-phase value;[20] thus, the MP2/aug-cc-pvDz level polarizability of an isolated Cl^- is essentially the same as the Cl^- anion polarizability in a condensed phase such as water. On the basis of this observation, we also adopt the MP2/aug-cc-pvDz and B3LYP/aug-cc-pvDz levels for estimating the polarization energies of anions complexed with the Li^+ cation.

The Li^+ binding energies to carbonates, ethers, and $TFSI^-$ anion were calculated at MP2, B3LYP, and Hartree−Fock (HF) levels using the aug-cc-pvDz basis set for solvent/anion, as shown in Table 1. The Gaussian 98 package[21] was used for all quantum chemistry calculations. Basis-set superposition-error (BSSE) correction was performed using the counterpoise method of Boys and Bernardi.[22] Binding energy is defined as the energy of the complex minus the energy of isolated optimized reactants. The nonbonded part of the binding energy is defined as the energy of the complex minus the energy of reactants using their geometry in the complex, and therefore, it does not include the solvent distortion energy. Table 1 reveals that the BSSE-corrected binding energies from MP2 calculations with full electron correlation are within 0.4 kcal/mol of the energies from the frozen core MP2(fc) calculations without BSSE correction because of insignificant electron correlations between core Li^+ electrons and solvent electrons. Therefore, a cheaper MP2(fc) level with no BSSE correction will be used in further studies instead of a more expensive MP2(full) method. The Li^+/solvent and Li^+/anion binding energies calculated at the MP2/aug-cc-pvDz level are systematically lower than the binding energies from the B3LYP and HF levels using the same basis sets. The nonbonded contributions to the binding energies always follow the trend MP2 < B3LYP < HF for the magnitude of the binding energy. A higher Li^+/solvent exchange−repulsion at the MP2/aug-cc-pvDz level compared to the B3LYP/aug-cc-pvDz and HF/aug-cc-pvDz levels and slightly smaller dipole moment of solvent molecules (see Table 2) are responsible for MP2 level calculations yielding lower solvent/Li^+ binding energies compared to the those from calculations at the B3LYP and HF levels. The binding energies in Table 1 have the following order: ether < DMC < DMK < EC < GBL < DME, whereas total binding energy normalized per a molecular volume in liquid solvent (not shown) has a different order: DMC < triglyme ≈ DME ≈ ether ≈ DMK < GBL < EC.

Finally, we note a large difference between the binding energies from our calculations and earlier low-level calculations. The most significant deviation of 20% is observed between the $Li^+(EC)_2$ binding energy of −101.1 kcal/mol calculated by Balbuena's group[7] at B3LYP/6-31G** level and our most accurate calculation of −83.74 kcal/mol obtained at the MP2/aug-cc-pvDz level, indicating large errors in estimating binding energies using small basis sets and B3LYP theory.

To fit Li^+/solvent and Li^+/anion repulsion parameters, the Li^+ binding energy to EC, acetone, DMC, ether, DME, and GBL was calculated as a function of separation at the MP2(fc)/aug-cc-pvDz level for low-energy path and the less computationally demanding B3LYP/aug-cc-pvDz level for higher-energy path, as shown in Figure 1.

TABLE 1: BSSE-Corrected Binding Energies and BSSE Corrections in Parentheses for Li^+ Complexes with Ethers, Carbonates, and $TFSI^-$

complex	MP2(full)/Dz	MP2(fc)/Dz	B3LYP/Dz	HF/Dz
		Total Binding Energy		
EC/Li^+	−47.8[a] (0.7)	−46.9 (0.6)	−51.8[b] (0.2)	−53.1[b] (0.1)
EC_2/Li^+	−83.7[a] (1.6)			−93.1[a] (0.4)
DMK/Li^+	−44.1[a] (0.6)	−43.2[a] (0.5)	−48.5[b] (0.2)	−48.9[c] (0.2)
ether/Li^+	−38.1[a] (0.8)	−37.2[a] (0.8)	−39.7[b] (0.2)	−39.3[c] (0.1)
DME/Li^+	−61.7[a] (1.5)			−63.7[c] (0.2)
triglyme/Li^+	−96.5[b] (2.1)		−96.7[b] (0.7)	−94.3[b] (0.5)
DMC/Li^+		−41.3		−44.5
GBL/Li^+		−48.7		−54.8
$TFSI^-$/Li^+		−134.5[d] (1.8)	−141.3[d] (0.4)	−141.3[d] (0.5)
		Nonbonded Part of Binding Energy		
EC/Li	−50.6	−49.7	−54.6	−56.0
EC_2/Li^+	−87.4			−95.5
ether/Li^+	−38.9	−38.0	−40.8	−41.4
DMK/Li^+	−44.6	−43.8	−49.4	−49.8
$TFSI^-$/Li^+		−140.9	−147.2	−146.3

[a] MP2/aug-cc-pvDz geometry. [b] B3LYP/aug-cc-pvDz geometry. [c] HF/aug-cc-pvDz geometry. [d] B3LYP/D95+(d,p) geometry.

TABLE 2: Solvent Dipole Moments from QC and MM and rms Deviation of Electrostatic Potential Predicted by Developed Force Field from That of the MP2/Aug-cc-pvDz Level

level of theory/basis set	DMC	GBL	DMK	EC	ether
Dipole Moment for Isolated Solvent Molecules (Debye)					
HF/aug-cc-pvDz//MP2/aug-cc-pvDz	0.42	5.34	3.41	5.97	1.51
B3LYP/aug-cc-pvDz//B3LYP/aug-cc-pvDz	0.43	4.80	3.11	5.51	1.27
MP2(fc)/aug-cc-pvDz//MP2(fc)/aug-cc-pvDz	0.31	4.69	2.99	5.38	1.36
MM using PET-FF (Debye) at MP2/aug-cc-pvDz geometries	0.19	4.53	2.85	5.38	1.38
Dipole Moment for Solvent Molecules Fixed at the Solvent/Li^+ Optimized Geometry					
MP2/aug-cc-pvDz dipole (Debye)	0.68[a]	5.15[a]	3.09[a]	6.15[a]	1.44[b]
MM dipole (Debye)	0.30	4.61	2.96	5.62	1.35
Quality of Electrostatic Potential Description					
isolated solvent geometry: ($\phi_i^{MM} - \phi_i^{MP2/aug-cc-pvDz}$) rms deviation (kcal/mol)	0.90	0.90	0.61	0.63	0.74
solvent geometry from the solvent/Li^+ complex: ($\phi_i^{MM} - \phi_i^{MP2/aug-cc-pvDz}$) rms deviation (kcal/mol)	1.38	1.50	0.67	1.27	1.0

[a] MP2/aug-cc-pvDz geometry. [b] B3LYP/aug-cc-pvDz geometry.

III. Force Field Development

A. Nonbonded Interactions. The Li^+/solvent interactions consist of repulsion/dispersion, Coulomb, and polarization contributions as given by eq 1.

$$U^{NB}(\mathbf{r}) = U^{RD}(\mathbf{r}) + U^{coul}(\mathbf{r}) + U^{pol}(\mathbf{r}) = A_{ij}\exp(-B_{ij}{*}r) + C_{ij}r^{-6} + \frac{1}{2}\sum_i\sum_j \frac{q_iq_j}{4\pi\epsilon_0 r_{ij}} - \sum_i \mu_i{\cdot}\boldsymbol{E}_i^0 - 0.5\sum_i\sum_j \mu_i{\cdot}\boldsymbol{T}{\cdot}\mu_j + \sum_i(\mu_i{\cdot}\mu_i/2\alpha_i) \quad (1)$$

where induced dipoles $\mu_i = \alpha_i \boldsymbol{E}_{tot}$, α_i is the isotropic atomic polarizability, $\boldsymbol{E}_{tot}$ is the total electrostatic field at the atomic site i due to permanent charges q_j and induced dipoles, ϵ_0 is the dielectric permittivity of vacuum, $\boldsymbol{E}_i^0$ is the electric field due to partial charges only, $\boldsymbol{T}_{ij}$ is the second-order dipole tensor, A_{ij} and B_{ij} are repulsion parameters, and C_{ij} are dispersion parameters.

The first two interactions are determined by charges and atomic polarizabilities reported in the previous paper for solvent molecules,[16] leaving only the repulsion/dispersion parameters and Li^+ polarizability to be determined here. An absence of the valence electrons and small core of a Li^+ cation leads to a very small polarization of Li^+ equal to 0.0285 $Å^{-3}$ from ref 23, suggesting that the Li^+/Li^+ dispersion interactions are small as estimated using London formula (eq 2)

$$C_{Li^+-Li^+} = -0.75\, IP_{Li}\alpha_{Li^+}{}^2 = 1.06 \text{ kcal mol}^{-1}\text{ Å}^{-6} \quad (2)$$

where IP is the ionization potential and α_{Li^+} is the polarizability of Li^+. We used values of $IP_{Li^+} = 1744.29$ kcal/mol[24] and $\alpha_{Li^+} = 0.0285$ $Å^{-3}$.[23] The force field Li^+−solvent dispersion cross terms were estimated using geometric mean combining rules and previously developed solvent and anion parameters.[16] The dispersion energies estimated from molecular mechanics (MM) calculations using a developed force field were 0.5−0.8 kcal/mol for the optimized complexes of Li^+ with ether, DMK, and EC. The dispersion energy calculated from the difference between the BBSE-corrected MP2(full) and MP2(fc) energies was 0.8−0.9 kcal/mol (see Table 1), indicating good agreement between the quantum chemistry estimates and MM results using developed force field for this small contribution to the Li^+/solvent binding energy.

At the next step, we fitted repulsion parameters to total energies of the Li^+/solvent binding energies along the path shown in Figure 1. These paths were generated by performing the optimization of the Li^+/solvent complex geometry at the MP2/aug-cc-pvDz level and shifting the Li^+ cation along a line schematically indicated in Figure 1 without reoptimizing solvent geometry. The C/Li^+ and H/Li^+ repulsion parameters were fitted to energies of the CH_4/Li^+ clusters. The O/Li^+ repulsion parameters were fit to the DMC/Li^+ and EC/Li^+ nonbonded part of the binding energy with the C/Li^+ and H/Li^+ parameters fixed to those previously determined by fitting the CH_4/Li^+ binding energies. The transferability of these parameters to ethers and other carbonates was checked by comparing the GBL/Li^+, ether/Li^+, and DME/Li^+ nonbonded binding energies calculated along paths shown in Figure 1b,d−f. The F/Li^+ repulsion parameters were fit to binding energies for CF_4/Li^+. The S/Li^+ and N/Li^+ repulsion parameters were fit to $TFSI^-$/Li^+ binding energies as shown in Figure 1g after atomic polarizabilities of S, N, and O were fit to reproduce $TFSI^-$ polarization energy due to the test unit (+1e) charge located along the same paths.[25] The Li^+/X, X = [O,C,F,N,S] repulsion parameters are summarized in Table 3. Combining rules were not applied during the fitting of the Li^+/X repulsion parameters but were used to obtain all repulsion−dispersion parameters for $TFSI^-$/solvent interactions from parameters reported in the previous paper.[16]

The Li^+/ethers and Li^+/cabonate binding energies at large (>2.5 Å) Li^+/solvent separations from MM calculations using developed force field are systematically lower than the binding energies from quantum chemistry calculations, as seen in Figure 1. This deficiency of the force field is somewhat puzzling because the force field accurately reproduces polarization energy and electrostatic potential around isolated solvent molecules at the optimized geometry and exchange−repulsion is insignificant at large separations. Closer examinations of the Coulomb, polarization, and repulsion contributions to the Li^+/ether and Li^+/carbonates binding energies revealed that the systematic underestimation of the binding energies in MM calculations at large Li^+/solvent separations is attributed to the failure of the force field to accurately reproduce a change in the solvent dipole moment and electrostatic potential around a solvent molecule due to geometry changes occurring upon Li^+ complexation. Table 2 summarizes dipole moments of ether and carbonates solvents calculated at the solvent/Li^+ complex geometry and isolated solvent geometry (no Li^+ present). A significant increase of the solvent dipole moment (up to 0.8 D) upon complexation with a Li^+ cation is observed in quantum chemistry calculations, whereas the corresponding increase of the solvent dipole moment is much smaller (only up to 0.35 D) in MM calculations with the developed force field. The force field also does an inferior job in describing the electrostatic potential around

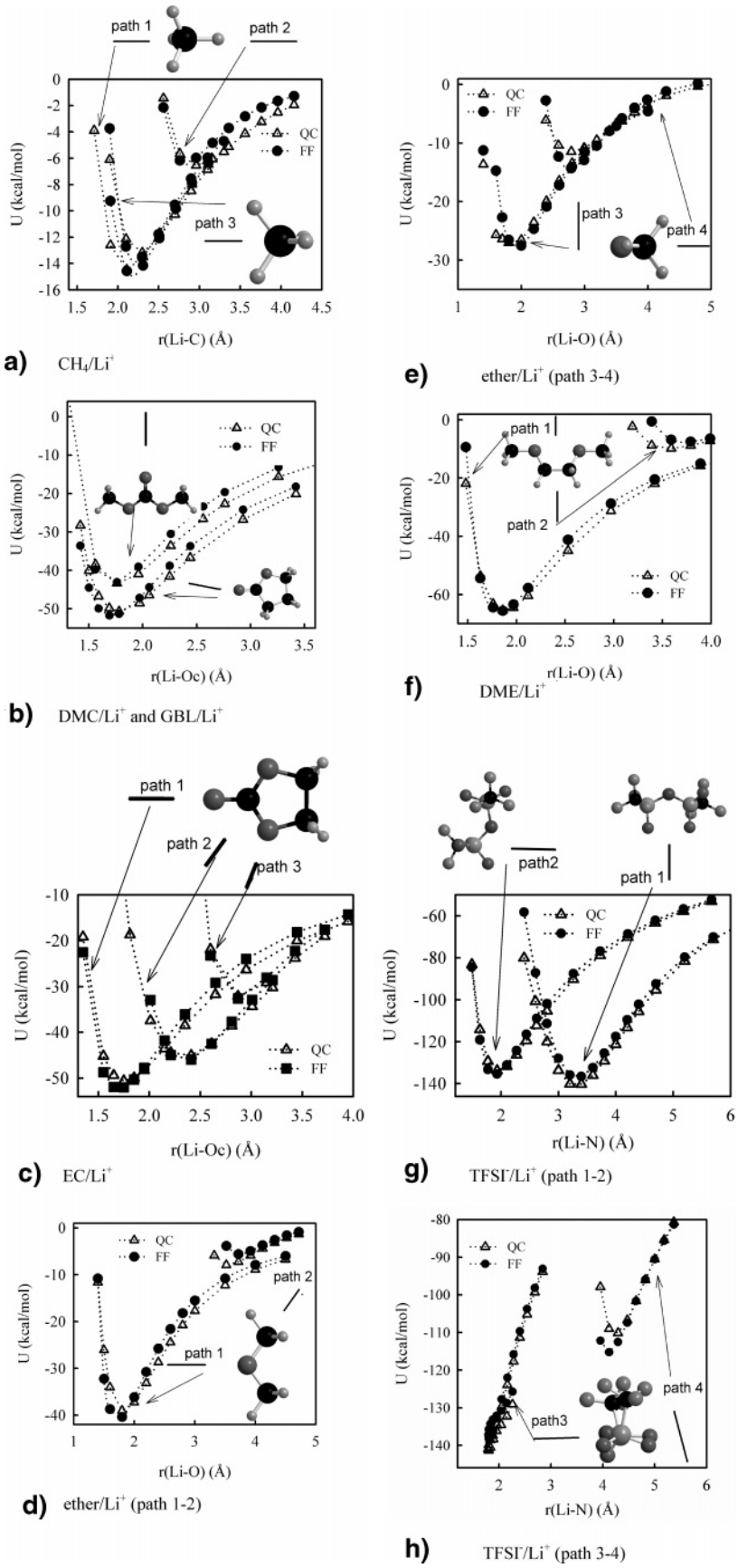

Figure 1. Total binding energy of Li^+ to solvent molecules and $TFSI^-$ anion.

solvent molecules taken from the solvent/Li^+ geometry compared to the description of isolated solvent geometries as shown in Table 2.

If an inability of the force field to reproduce changes in the solvent dipole moment with molecular geometry upon solvent/Li^+ complexation is indeed responsible for the difference

TABLE 3: Li^+/Solvent and Li^+/$TFSI^-$ Repulsion−Dispersion Parameters

atom types	A (kcal mol^{-1})	B (Å^{-1})	C (kcal Å^{-6} mol^{-1})
Li−Li	44195.0	7.2770	1.06
Li−H	37404.5	5.3341	5.59
Li−C_m[a]	95861.2	4.3460	19.94
Li−C	95861.2	4.3460	18.77
Li−C_c[b]	95861.2	4.3460	23.02
Li−N	15700.0	3.6717	25.64
Li−O	49530.0	4.4757	18.13
Li−F	32368.0	4.8200	13.19
Li−S	48196.0	3.4800	37.18

[a] C_m, methoxy carbon. [b] C_c, carbonyl group carbon.

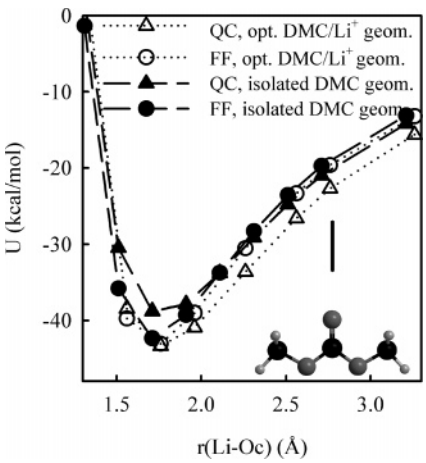

Figure 2. Total DMC/Li^+ binding energy for complexes with DMC molecule using geometry from the optimized DMC/Li^+ complex and the isolated gas-phase DMC geometry.

between the Li^+/solvent binding energetics from MM and quantum chemistry calculations, then the force field should accurately predict solvent/Li^+ binding energies at large separations for the solvent/Li^+ complexes where solvent geometry was not optimized, i.e., corresponding to the isolated solvent geometry. Figure 2 compared the Li^+/DMC binding energy for the same path but two different geometries of a DMC molecule: (a) the DMC geometry taken from the fully optimized Li^+/DMC complex and shifted relative to a Li^+ as in Figure 1; (b) the DMC geometry taken from the optimization of an isolated DMC molecule and frozen during calculation of DMC/Li^+ binding energies. The Li^+/DMC binding energy for the complex with the isolated DMC geometry was accurately described by the force field at large separations supporting the above arguments that deviation of the solvent/Li^+ binding energies from MM calculations from quantum chemistry at large separations is indeed due to the poor ability of the force field to describe changes of the dipole moment upon solvent geometry distortion by a Li^+. Figure 2 also indicates that at close Li^+/DMC contact, where solvent geometry is expected to be significantly deformed, MM calculations are in agreement with quantum chemistry results for the optimized DMC/Li^+ geometry, whereas at large separations, where solvent geometry is expected to be similar to the isolated DMC geometry, the results of MM calculations agree nicely with the quantum chemistry results for the DMC/Li^+ complex that contains a DMC molecule in the isolated geometry.

B. $TFSI^-$ Intramolecular Force Field. The total energy of the $TFSI^-$ anion in a classical force field is given by a sum of the nonbonded contributions (eq 1), and the intramolecular energy due to bends and torsions is given by eq 3.

$$U^{\mathrm{tot}}(\mathbf{r}) = \sum_{i<j} U^{\mathrm{NB}}(r_{ij}) + {}^1/_2 k^{\mathrm{BEND}}_{\alpha\beta\gamma}(\theta_{ijk} - \theta^0_{\alpha\beta\gamma})^2 + \sum_n {}^1/_2 k^{\mathrm{t}}_{\alpha\beta\gamma\delta}(n)[1 - \cos(n\phi_{ijkl})] \quad (3)$$

Energy due to bonds is not included in eq 3 because bond lengths are constrained in the force field. Bend force constants were taken from ref 26, where they were fitted to virbrational frequencies of the $TFSI^-$ anion. Equilibrium bond length and bend angles were fit to $TFSI^-$ geometry optimized at the B3LYP/aug-cc-pvDz level. The F−C−S−N and C−S−N−S torsions were fit to energies of CF_3 group rotation and C−S−N−S torsional drives, respectively, calculated at the MP2/aug-cc-pvDz//B3LYP/D95+* level.

IV. Simulation Results and Discussion

MD simulations methodology is described in the previous paper.[16] All liquid electrolytes were simulated for at least one solvent/Li^+ and anion/Li^+ residence time to ensure multiple exchange of solvent/anion molecules in the Li^+ environment. Simulation times for liquid/electrolytes such as DME/LiTFSI, DMC/LiTFSI, PC/LiTFSI, and EC/LiTFSI were 2−10 ns depending on temperature, whereas much longer simulations of 15−45 ns were performed for PEO (MW = 2380)/LiTFSI. Electrolytes contained between 3000 and 5500 force centers and included at least 8 LiTFSI molecules for the most dilute cases simulated.

A. Thermodynamic Properties. The density of electrolytes significantly increases with increasing LiTFSI salt concentration. The ability of MD simulations to predict an electrolyte density increase over wide concentration range is demonstrated in Figure 3 for PC/LiTFSI and DME/LiTFSI. The apparent molar volume is more sensitive to solvent/salt interactions compared to the overall density. MD simulation predictions of apparent molar volume are in good agreement with the experiments for the PC/LiTFSI and DME/LiTFSI electrolytes, as seen in Figure 4. We note that neither overall density nor apparent molar volumes of LiTSFI were included in force field parametrization; therefore, the data in Figure 4 constitute MD simulation predictions using Li^+/solvent, Li^+/$TFSI^-$ quantum chemistry data, and combining rules for the $TFSI^-$/solvent interactions.

B. Structure. The Li^+ cation environment in PEO/LiTFSI, EO−Li = 7.5:1 was carefully studied in the recent neutron diffraction isotopic substitution (NDIS) experiments at 296 K.[27] NDIS experiments found the first Li−O peak at 2.1 ± 0.05 Å and 4.9 ether oxygen atoms in the first coordination of Li^+ obtained by fitting the experimental pair-distribution function with the Gaussian. MD simulations at 393 K for the same salt concentration predicted the position of the first Li−O peak was 1.97 Å in good agreement with experimental value of 2.1 ± 0.05 Å. The number of ether oxygen atoms around a Li^+ cation was 4.6 using 2.8 Å cutoff in close agreement with 4.9 ether oxygen atoms from experiments. More details about ion structure and aggregation in PEO/LiTFSI are presented elsewhere.[28]

C. Transport Properties. Ion self-diffusion coefficients were calculated from MD simulations as a slope of mean-squared displacements vs time divided by six. The conductivity (λ) was calculated using the Einstein relation for liquid electrolytes using eq 4

$$\lambda = \lim_{t\to\infty} \frac{e^2}{6tVk_{\mathrm{B}}T} \sum_{ij}^{N} z_i z_j \langle [\boldsymbol{R}_i(t) - \boldsymbol{R}_i(0)][\boldsymbol{R}_j(t) - \boldsymbol{R}_j(0)] \rangle \quad (4)$$

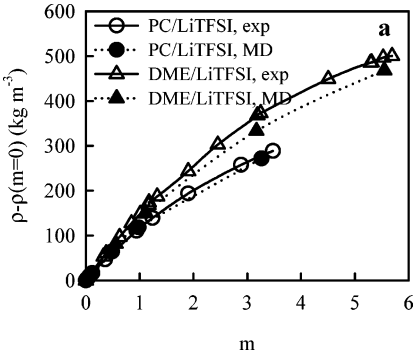

Figure 3. Density increase relative to pure solvents of DME/LiTFSI at 308 K and PC/LiTFSI at 298 K from experiments[29] and MD simulations.

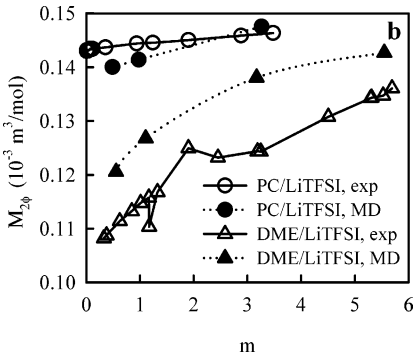

Figure 4. Apparent molar volumes of DME/LiTFSI at 308 K and PC/LiTFSI at 298 K from experiments[29] and MD simulations.

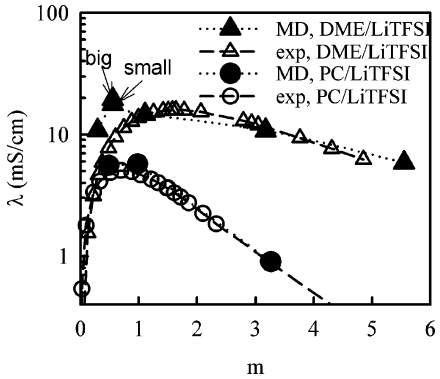

Figure 5. Specific conductivity of DME/LiTSI at 308 K and PC/LiTFSI at 298 K electrolytes from experiments[29] and MD simulations.

where e is the electron charge, V is the volume of the simulation box, k_B is the Boltzmann's constant, T is the temperature, t is time, z_i and z_j are the charges over ions i and j in electrons, $\boldsymbol{R}_i(t)$ is the displacement of the ion i during time t, the summation is performed over all ions, $\langle\ \rangle$ denote the ensemble average, and N is the total number of ions in the simulation box.

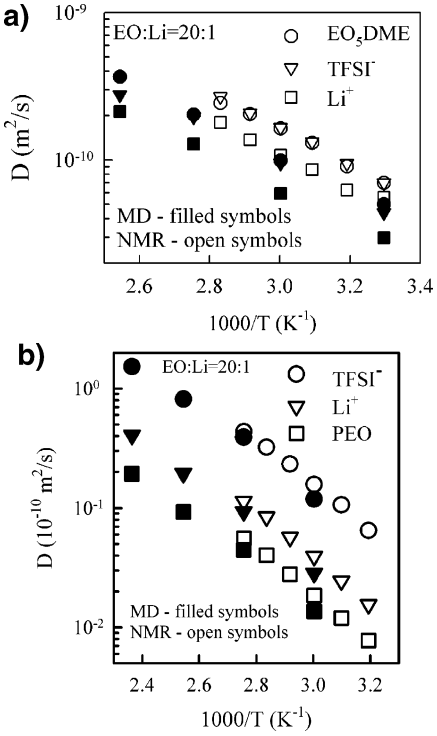

Figure 6. Self-diffusion coefficients of ions and solvent for (a) pentaglyme/LiTFSI and (b) PEO/LiTFSI at EO−Li = 20:1 from MD simulations and NMR experiments.[30] See ref 28 on details on LiTFSI transport in PEO/LiTFSI.

The degree of decorrelated ion motion (α) is typically measured as a ratio of the collective (total) charge transport to the charge transport due to self-diffusion only (a limit of completely dissociated and uncorrelated motion) and is frequently expressed as

$$\lambda = \alpha N e^2 (D_+ + D_-)/V k_B T \tag{5}$$

Equation 5 was used to obtain the degree of ion correlation from a combination of pgf-NMR and conductivity measurements.[31]

The conductivities of DME/LiTFSI and PC/LiTFSI were calculated from MD simulations over a broad concentration range and are compared with experiments[29] in Figure 5. MD simulations accurately predicted PC/LiTFSI conductivity over the whole concentration range, whereas in DME/LiTFSI, the conductivity maximum was predicted at lower concentrations than experimentally observed. Two DME/LiTFSI electrolytes of different sized system were simulated for $m = 0.56$ (DME−Li = 20:1) to check for finite size effects on ion aggregation and transport properties: a small system containing 9 LiTFSI and a larger one containing 17 LiTFSI. Conductivity (Figure 5), ion self-diffusion coefficients, and degree of ion dissociation

TABLE 4: Solvent and Ion Self-Diffusion Coefficients from MD Simulations and pgf-NMR Experiments[31] at 303 K

solvent	number of Li^+ in a simulation cell	$D^{solvent}$ (10^{-10} m²/s)	D^{TFSI^-} (10^{-10} m²/s)	D^{Li^+} (10^{-10} m²/s)	α	error 100% $(X^{MD} - X^{exp})/X^{exp}$ solvent	TFSI⁻	Li^+
DME[a]	17	20.9 (22)	7.7 (8.8)	10.5 (7.7)	0.63 (0.31)	−5	−12	36
DME[a]	9	19.1 (22)	7.4 (8.8)	10.0 (7.7)	0.60 (0.31)	−13	−16	29
EC	20	5.8 (4.3)	2.9 (3.1)	2.9 (2.1)	0.76 (0.67)	35	−6	39
EC[b]	10	5.5 (4.3)	2.9 (3.1)	2.8 (2.1)	0.79 (0.67)	27	6	35
PC	8	2.82 (3.5)	1.41 (2.6)	1.25 (1.6)	0.8 (0.62)	−19	−46	−22
DMC	10	11.2 (16)	3.75 (6.0)	3.21 (5.8)	0.19 (0.11)	−30	−38	−45

[a] MD simulations of DME/LiTFSI were performed at 308 K, reported self-diffusion coefficients were reduced by 6% to account for temperature dependence between 308 and 303 K. [b] Results at 313 K are reported for EC/LiTFSI.

(α) shown in Table 4 were found independent of the size of the simulation cell (box).

The ability of MD simulations to predict the ion and solvent self-diffusion coefficient as a function of temperature was tested on pentaglyme(EO_5DME)/LiTFSI and PEO/LiTSFI electrolytes (see Figure 6). Ion and pentaglyme self-diffusion coefficients from MD simulations were ≈40−50% slower than experiments,[30] whereas ion self-diffusion coefficients in PEO/LiTFSI were within 20% of experimental measurements.[30] The pgf-NMR measurements[31] were also performed on EC, PC, DME, and DMC doped with LiTFSI at solvent−salt molar ratios of 20:1. The solvent and ion self-diffusion coefficients from MD simulations are compared with those from pgf-NMR[31] in Table 4. The solvent self-diffusion coefficients were predicted with a maximum deviation of 35% from experiments, whereas ion self-diffusion coefficients from MD simulations were within 46% of experiments. More importantly, MD simulations accurately predict the degree of ion decorrelated motion (α) for EC, PC, and DMC, also shown in Table 4. The degree of uncorrelated motion for dilute DME/LiTFSI is overestimated in our MD simulations and is responsible for higher conductivities of DME/LiTFSI as low salt concentrations shown in Figure 5. Overall, we are satisfied with the obtained agreement of transport properties from MD simulations and experiments.

Conclusions

Quantum chemistry-based many-body polarizable force fields have been derived for the oligoether, linear carbonate, and cyclic carbonate electrolytes doped with LiTFSI salt. We found that relatively large basis sets such as aug-cc-pvDz for solvents and [8s4p3d/5s3p2d] for Li^+ need to be used to accurately estimate the Li^+/solvent and $Li^+/TFSI^-$ binding energies. Usage of B3LYP/6-31G** basis sets with no BSSE correction could lead to errors up to 20% in estimating Li^+/solvent interactions.

MD simulations with developed force fields provided good and reliable predictions of the Li^+ cation complexation environment, electrolyte density, conductivity, and ion and solvent self-diffusion coefficients for concentrations from dilute to very concentrated and for temperatures from room temperature to 423 K. The developed force field is accurate and reliable enough to use for studies aimed at obtaining a fundamental understanding of ion transport and design novel electrolytes aimed at Li-battery applications.

Acknowledgment. We are indebted to subcontract from LBL #6515401 and NASA (Grant NAG3 2624) for financial support.

References and Notes

(1) *HandBook of Battery Materials*; Besenhard, J. O., Ed.; Wiley-VCH: New York, 1999.
(2) Kim, Y.-T.; Smotkin, E. S. *Solid State Ionics* **2002**, *149*, 29−37.
(3) Tarascon, J.-M.; Armand, M. *Nature* **2001**, *414*, 359−367.
(4) Abraham, K. M. In *Applications of Electroactive Polymers*; Scrosati, B., Ed.; Chapman & Hall: London, 1994; p 75.
(5) Abraham, K. M.; Jiang, Z.; Carroll, B. *Chem. Mater.* **1997**, *9*, 1978−1988.
(6) Stallworth, P. E.; et al. *J. Power Sources* **1999**, *81*, 739.
(7) Masia, M.; Rey, R. *J. Phys. Chem. B* **2004**, *108*, 17992.
(8) Soetens, J.-C.; Millot, C.; Maigret, D. *J. Phys. Chem. A* **1998**, *102*, 1055.
(9) Hyunm J.-K.; Dong, H.; Rhodes, C. P.; Frech, R.; Wheeler, R. A. *J. Phys. Chem. B* **2001**, *105*, 3329.
(10) Tasaki, K. *J. Electrochem. Soc.* **2002**, *149*, A418.
(11) Newman, J.; Thomas, K. E.; Hafezi, H.; Wheller, D. R. *J. Power Sources* **2003**, *119*−*121*, 838−843.
(12) Müller-Plather, F.; van Gunsteren, W. F. *J. Chem. Phys.* **1995**, *103*, 4745.
(13) Mos, B.; Verkerk, P.; Pouget, S.; van Zon, A.; Bel, G.-J.; de Leeuw, S. W.; Eisenbach, C. D. *J. Chem. Phys.* **2000**, *113*, 4.
(14) Borodin, O.; Smith, G. D. Molecular Modeling of Poly(Ethylene Oxide) Melts And Poly(Ethylene Oxide)-Based Polymer Electrolytes. In *Methods and Applications in Computational Materials Chemistry*; Curtiss, L., Gordon, M., Eds.; Kluwer Academic Publishers: Boston, MA, 2004; pp 35−90.
(15) Borodin, O.; Smith, G. D. *Macromolecules* **2000**, *33*, 2273−2283.
(16) Borodin, O. Smith, G. D. *J. Phys. Chem. B* **2006**, Previous paper of this issue.
(17) Smith, G. D.; Jaffe, R. L.; Partridge, H. *J. Phys. Chem. A* **1997**, *101*, 1705.
(18) Anisimov, V. M.; Lamoureux, G.; Vorobyov, I. V.; Huang, N.; Roux, B.; MacKerell, A. D. *J. Chem. Theory Comput.* **2005**, *1*, 153.
(19) Woon, D. E.; Dunning, T. H., Jr. *J. Chem. Phys.* **1994**, *100*, 2975−2988.
(20) Morita, A.; Kato, S. *J. Chem. Phys.* **1999**, *110*, 11987−11998.
(21) Frisch, M. J.; Trucks, G. W.; Schlegel, H. B.; Scuseria, G. E.; Robb, M. A.; Cheeseman, J. R.; Zakrzewski, V. G.; Montgomery, J. A., Jr.; Stratmann, R. E.; Burant, J. C.; Dapprich, S.; Millam, J. M.; Daniels, A. D.; Kudin, K. N.; Strain, M. C.; Farkas, O.; Tomasi, J.; Barone, V.; Cossi, M.; Cammi, R.; Mennucci, B.; Pomelli, C.; Adamo, C.; Clifford, S.; Ochterski, J.; Petersson, G. A.; Ayala, P. Y.; Cui, Q.; Morokuma, K.; Malick, D. K.; Rabuck, A. D.; Raghavachari, K.; Foresman, J. B.; Cioslowski, J.; Ortiz, J. V.; Stefanov, B. B.; Liu, G.; Liashenko, A.; Piskorz, P.; Komaromi, I.; Gomperts, R.; Martin, R. L.; Fox, D. J.; Keith, T.; Al-Laham, M. A.; Peng, C. Y.; Nanayakkara, A.; Gonzalez, C.; Challacombe, M.; Gill, P. M. W.; Johnson, B. G.; Chen, W.; Wong, M. W.; Andres, J. L.; Head-Gordon, M.; Replogle, E. S.; Pople, J. A. *Gaussian 98*, revision A.7; Gaussian, Inc.: Pittsburgh, PA, 1998.
(22) Boys, S. F.; Bernardi, F. *Mol. Phys.* **1970**, *19*, 553−556.
(23) *Reference Data on Atoms, Molecules and Ions*; Radzig, A. A., Smirnov, B. M., Eds.; Springer-Verlag: Berlin, Germany, 1985.
(24) *CRC Handbook*, 81st ed.; CRC Press: Boca Raton, FL, 2000.
(25) Partial charges for atoms of the TFSI−anion were fit to an electrostatic grid calculated at the MP2(fc)/aug-cc-pvDz level.
(26) Rey, I.; Johansson, P.; Lindgren, J.; Lassègues, J. C.; Grondin, J.; Servant, L. *J. Phys. Chem. A* **1998**, *102*, 3249−3258.
(27) Moa, G.; Saboungi, M.-L.; Price, D. L.; Armand, M. B.; Howells, W. S. *Phys. Rev. Lett.* **2000**, *84*, 5536.
(28) Borodin, O.; Smith, G. D. *Macromolecules* **2006**, *39*, 1620.
(29) Brouillette, D.; Perron G.; Desnoyers, J. E. *J. Solution Chem.* **1998**, *27*, 151.
(30) Hayamizu, K.; Akiba, E.; Bando, T.; Aihara, Y. *J. Chem. Phys.* **2002**, *117*, 5929.
(31) Hayamizu, K.; Aihara, Y.; Arai, S.; Martinez, C. G. *J. Phys. Chem. B* **1999**, *103*, 519.